SCIREA Journal of Environmental

http://www.scirea.org/journal/Environmental

October 29, 2016

Volume 1, Issue1, October 2016

Refined Numerical Simulation of Environmental Flow, Mixing and Transport in Amazon River near Manaus City by Using Multiple Depth-Averaged Two-Equation Turbulence Models and Multi-Grid Iterative Method

Li-ren Yu[1,2] and Jun Yu[3]

1. ESDV (Environmental Software and Digital Visualization), Rm.302, Unit4, Building420, Wan-Sheng-Bei-Li, Ton-Zhou Dist., 101121, Beijing, China.

2. ASSER-CESUSC (Association of United Schools-Higher Education Center at São Carlos), Brazil.

E-mail: *lirenyu@yahoo.com*.

3. Lenovo, Av. Carlos Grimaldi, 1701, 2^0 andar/Campins – SP, Brazil

Abstract

This paper reports a refined numerical simulation for Amazon River, aiming to develop a mathematical model and numerical tool for modeling and predicting turbulence flows and contaminant transport in complex natural waters. In the mathematical model, the depth-averaged two-equation closure turbulence $\tilde{k}-\tilde{\omega}$ model, together with $\tilde{k}-\tilde{\varepsilon}$ model and $\tilde{k}-\tilde{w}$ model, were used to close non-simplified quasi 3D hydrodynamic fundamental governing equations. The discretized equations, however, were solved by advanced multi-grid iterative method under coarse and fine two-levels' non-orthogonal body-fitted grids with collocated variable arrangement. Except for steady flow and transport computation, the processes of black-water inpouring and plume development, caused by the side-discharge from the Negro

River, also have been numerically studied. The used three depth-averaged two-equation closure models are suitable for modeling strong mixing turbulence. The recently built $\tilde{k}-\tilde{\omega}$ turbulence model with higher order of magnitude of transported variable $\tilde{\omega}$ provides a possibility to enhance the computational precision. Based on the developed mathematical model, which can provide multiple turbulence two-equation closure models for quasi 3D modeling, a CFD software, namely **Q3drm1.0** and **Q3drm2.0**, was developed. This numerical tool focuses on the refined numerical simulations of the steady and unsteady problems of flow and transports with the strong ability to deal with different tipes of discharges. In this paper, only the investigation of side-discharge is presented.

Key words: depth-averaged turbulence models, river modeling, contaminant transport, turbulent mixing, grid generation with multiple islands, multi-grid iterative method

1 Introduction

Almost all flows in natural waters are turbulence. Dealing with the problems of turbulence, related tightly to stream pollutions, is challenging both for scientists and engineers, because of their damaging effect on our fragile environment and limited resources. It is important to develop adequate mathematical models, turbulence closure models, numerical methods and corresponding analytical tools for timely simulating and predicting contaminant transport behaviors in natural waters.

Although the significance of modeling turbulent flows and contaminant transport phenomena with a high precision is clear, the numerical simulation and prediction for natural waters with complex geometry and various islands as well as variable bottom topography are still unsatisfied. This is mainly due to the inherent complexity of the problems being considered. Any computation of flow and transport processes depends critically on following four elements: to generate a suitable computational domain with the ability to deal with non-regular geometrical boundaries, such as riversides and island boundaries; to establish applicable turbulence closure models; to adopt efficient algorithms, and to develop corresponding numerical tool, respectively.

Numerous environmental flows can be considered as shallow, *i.e.*, the horizontal length scales of the flow domain are much larger than the water-depth. Typical examples are found in open

channels, rivers, reservoirs and lakes, estuaries and coastal regions, oceanic and even in stratified atmospheric flows. Depth-averaged mathematical models are frequently used for modelling the flow and contaminant transport in well-mixed shallow waters. However, many models used in practice merely consider the depth-averaged turbulent viscosity and diffusivity through constants or through simple phenomenological algebraic formulas [1-3], which are to a great degree estimated according to the modeller's experience. Although some practical quasi 3D hydrodynamic models are really closed by depth-averaged two-equation closure turbulence model, they almost all concentrate on the investigations and applications of depth-averaged $\widetilde{k}-\widetilde{\varepsilon}$ model [4-7], which appeared already beyond 30 years. It is well known that the order of magnitude of transported variable $\widetilde{\varepsilon}$ for $\widetilde{k}-\widetilde{\varepsilon}$ model is very low indeed.

Recent development of turbulence model theory has provided more realistic closure models, such as DNS, LES and RANS-based models, *etc* [8]. However, from an engineering perspective, one class of RANS-based models, *i.e.* two-equation closure turbulence models, can build a higher standard for numerically approximation of main flow behaviors and transport phenomena in terms of efficiency, extensibility and robustness. Unfortunately, the 'standard' two-equation closure models, used widely in industry, cannot be directly employed in quasi 3D modeling, and corresponding depth-averaged models should be built in advance.

Except for the depth-averaged $\widetilde{k}-\widetilde{\omega}$ model closure, recently built by the author, present simulations still adopt the closure approaches of classical depth-averaged $\widetilde{k}-\widetilde{\varepsilon}$ model and depth-averaged $\widetilde{k}-\widetilde{w}$ model, respectively. It is well known that the depth-averaged $\widetilde{k}-\widetilde{\omega}$ model was stemmed from the most common 'standard' k-ω model, originally introduced by Saffman [9] and popularized by Wilcox [10]. In this paper, the results, computed by the three depth-averaged two-equation turbulence models, mentioned above, were compared each other. Such example, however, hardly exists for the simulation of contaminant transport in natural waters. Modeling by using different two-equation closure approaches will certainly increase the credibility of users' calculated results.

On the other hand, recent advancements in grid generation techniques, numerical methods and IT techniques have provided suitable approaches to generate non-orthogonal boundary-fitted coordinates with collocated grid arrangement, on which the non-simplified hydrodynamic fundamental governing equations can be solved by multi-grid iterative method [11]. This paper describes a quasi 3D hydrodynamic simulation of flow and contaminant transport in a multi-connected domain, with the aim to develop corresponding *grid-generator*, *flow-solver*

and *Graphical User Interface* (GUI). **Q3drm1.0** and **Q3drm2.0** software developed by the author provide three or five selectable depth-averaged two-equation closure turbulence models and can refinedly solve environmental flows and contaminant transport phenomena in natural and artificial waters with or without islands.

2 Hydrodynamic Fundamental Governing Equations

The complete fundamental governing equations of quasi 3D computation, in terms of coordinate-free vector forms derived by using vertical Leibniz integration for a Control Volume (CV, an arbitrary quadrilateral with center point *P*), considering the variation of the bottom topography and water surface and neglecting minor terms in the depth-averaging procedure, can be written as follows:

$$\frac{\partial}{\partial t}\int_{\Omega}\rho h\bar{\phi}d\Omega+\int_{S}\rho h\bar{\phi}\vec{v}\bullet\vec{n}dS=\int_{S}\Gamma h\mathbf{grad}\bar{\phi}\bullet\vec{n}dS+\int_{\Omega}\bar{q}_{\phi}d\Omega \qquad (1)$$

where Ω is the CV's volume; S is the face; $\vec{v}$ is the depth-averaged velocity vector; the superscript "$-$" indicates that the value is strictly depth-averaged; $\bar{\phi}$ is any depth-averaged conserved intensive property (for mass conservation, $\bar{\phi}=1$; for momentum conservation, $\bar{\phi}$ is the components in different directions of $\vec{v}$; for conservation of a scalar, $\bar{\phi}$ is the conserved property per unit mass); Γ is the diffusivity for the quantity $\bar{\phi}$; $\bar{q}_{\phi}$ denotes the source or sink of $\bar{\phi}$; and h and ρ are local water depth at P and density, respectively.

For the momentum conservation of Eq. (1), $\Gamma=\tilde{\mu}_{eff}$ (depth-averaged effective viscosity); for temperature or concentration transport, $\Gamma=\tilde{\Gamma}_{\phi,t}$ (temperature or concentration diffusivity), where the superscript "~" indicates the quantity characterizing depth-averaged turbulence. The source (sink) term $\bar{q}_{\phi}$ for momentum conservation may include surface wind shear stresses, bottom shear stresses, pressure terms and additional point sources (or point sinks).

3 Depth-Averaged Turbulence Closure Models

The depth-averaged effective viscosity $\tilde{\mu}_{eff}$ and diffusivity $\tilde{\Gamma}_{\phi,t}$, appeared in Eq. (1), are dependent on the molecular dynamic viscosity μ and depth-averaged eddy viscosity $\tilde{\mu}_t$:

$\tilde{\mu}_{eff} = \mu + \tilde{\mu}_t$ and $\tilde{\Gamma}_{\phi,t} = \tilde{\mu}_t / \sigma_{\phi,t}$, where $\sigma_{\phi,t}$ is the turbulence Prandtl number for temperature diffusion or Schmidt number for concentration diffusion, and $\tilde{\mu}_t$ is a scalar property and normally determined by two extra transported variables.

Recently, the author established a depth-averaged two-equation closure turbulence model $\tilde{k} - \tilde{\omega}$, based on the 'standard' k-ω model (in which ω is the special dissipation rate). The 'standard' k-ω turbulence model has been used in engineering researches [12]. In depth-averaged $\tilde{k} - \tilde{\omega}$ model, the turbulent viscosity is expressed by:

$$\tilde{\mu}_t = \rho \tilde{k} / \tilde{\omega} \tag{2}$$

where $\tilde{k}$ and $\tilde{\omega}$ stand for the depth-averaged turbulent kinetic energy and special dissipation rate of turbulence kinetic energy in the depth-averaged sense. They are determined by solving two extra transport equations, *i.e.*, the $\tilde{k}$-eq. and $\tilde{\omega}$-eq., respectively [13]:

$$\frac{\partial(\rho h\tilde{k})}{\partial t} + div(\rho h\tilde{k}\vec{v}) = div(h(\mu + \frac{\tilde{\mu}_t}{\sigma_k^*})\mathbf{grad}\tilde{k}) + hP_k - \rho\beta^* h\tilde{k}\tilde{\omega} + \rho h P_{kv} + \bar{S}_k \tag{3}$$

$$\frac{\partial(\rho h\tilde{\omega})}{\partial t} + div(\rho h\tilde{\omega}\vec{v}) = div(h(\mu + \frac{\tilde{\mu}_t}{\sigma_\omega^*})\mathbf{grad}\tilde{\omega}) + \alpha h\frac{\tilde{\omega}}{\tilde{k}}P_k - \rho h\beta\tilde{\omega}^2 + \rho h P_{\omega v} + \bar{S}_\omega \tag{4}$$

where $\bar{S}_k$ and $\bar{S}_\omega$ are the source-sink terms, $P_k = \tilde{\mu}_t\left[2\left(\frac{\partial\bar{u}}{\partial x}\right)^2 + 2\left(\frac{\partial\bar{v}}{\partial y}\right)^2 + \left(\frac{\partial\bar{u}}{\partial y} + \frac{\partial\bar{v}}{\partial x}\right)^2\right]$ is the production of turbulent kinetic energy due to interactions of turbulent stresses with horizontal mean velocity gradients. The values of empirical constants α, β, β^*, σ_k^*, and σ_ω^* in Eq. (3) through Eq. (4) are the same as in the 'standard' k-ω model: 5/9, 0.075, 0.9, 2, and 2, respectively. According to the dimensional analysis, the additional source terms P_{kv} in k-eq. (3) and $P_{\omega v}$ in ω-eq. (4) are mainly produced by the vertical velocity gradients near the bottom, and can be expressed as follows:

$$P_{kv} = C_k u_*^3 / h,\ P_{\omega v} = C_\omega u_*^2 / h^2 \tag{5}$$

while the local friction velocity u_* is equal to $\sqrt{C_f\left(\bar{u}^2 + \bar{v}^2\right)}$, the empirical constant C_ω for open channel flow and rivers can be expressed as:

$$C_\omega = \beta / (C_\mu \times e^* \times C_f{}^{1/2}) \tag{6}$$

where C_f represents an empirical friction factor and e^* is the dimensionless diffusivity of the empirical formula for undisturbed channel/river flows $\tilde{\mu}_t = e^* U_* h$ with U_* being the global friction velocity.

Except for the newly developed $\tilde{k}-\tilde{\omega}$ turbulence model mentioned above, the author also adopts depth-averaged $\tilde{k}-\tilde{\varepsilon}$ model and $\tilde{k}-\tilde{w}$ model, to close the fundamental governing equations in the current computations. The $\tilde{k}-\tilde{\varepsilon}$ model was suggested by McGuirk and Rodi [14] as early as in 1977:

$$\frac{\partial(\rho h\tilde{k})}{\partial t} + div(\rho h\tilde{k}\vec{v}) = div(h(\mu + \frac{\tilde{\mu}_t}{\sigma_k})\mathbf{grad}\tilde{k}) + hP_k - \rho h\tilde{\varepsilon} + \rho hP_{kv} + \bar{S}_k \qquad (7)$$

$$\frac{\partial(\rho h\tilde{\varepsilon})}{\partial t} + div(\rho h\tilde{\varepsilon}\vec{v}) = div(h(\mu + \frac{\tilde{\mu}_t}{\sigma_\varepsilon})\mathbf{grad}\tilde{\varepsilon}) + C_1 hP_k \frac{\tilde{\varepsilon}}{\tilde{k}} - C_2 \rho h \frac{\tilde{\varepsilon}^2}{\tilde{k}} + \rho hP_{\varepsilon v} + \bar{S}_\varepsilon \qquad (8)$$

where $\bar{S}_k$ and $\bar{S}_\varepsilon$ are the source-sink terms, $\tilde{\mu}_t$ can be expressed as:

$$\tilde{\mu}_t = \rho C_\mu \tilde{k}^2 / \tilde{\varepsilon} \qquad (9)$$

where $\tilde{\varepsilon}$ stands for dissipation rate of $\tilde{k}$. The values of empirical constants C_μ, σ_k, σ_ε, C_1 and C_2 in Eqs. (7-9) are the same as the 'standard' k-ε model, *i.e.* equal to 0.09, 1.0, 1.3, 1.44 and 1.92, respectively. The additional source terms P_{kv} and $P_{\varepsilon v}$ in Eqs. (7) and (8) can be written by:

$$P_{kv} = C_k u_*^3 / h,\ P_{\varepsilon v} = C_\varepsilon u_*^4 / h^2 \qquad (10)$$

where the empirical constants C_k and C_ε for open channel flow and rivers are:

$$C_k = 1/\sqrt{C_f},\ C_\varepsilon = C_2 C_\mu^{1/2} / (C_f^{3/4} \times e^{*1/2}) \qquad (11)$$

The third used depth-averaged second-order closure $\tilde{k}-\tilde{w}$ model was previously developed by the author of the present paper and his colleague [15]. This model originated from the revised k-w model developed by Ilegbusi and Spalding [16]. The two extra transport equations of this model (*i.e.*, the $\tilde{k}$-eq. and $\tilde{w}$-eq.) should be:

$$\frac{\partial(\rho h\tilde{k})}{\partial t} + div(\rho h\tilde{k}\vec{v}) = div(h(\mu + \frac{\tilde{\mu}_t}{\sigma_k})\mathbf{grad}\tilde{k}) + hP_k + \rho hP_{kv} - C_\mu \rho h\tilde{k}\tilde{w}^{1/2} + \bar{S}_k \qquad (12)$$

$$\frac{\partial(\rho h\tilde{w})}{\partial t}+div(\rho h\tilde{w}\vec{v})=div(h(\mu+\frac{\tilde{\mu}_t}{\sigma_\varepsilon})\mathbf{grad}\tilde{w})+C_{1w}\tilde{\mu}_t h(\mathbf{grad}\Omega)^2$$

$$-C_{2w}\rho h\tilde{w}^{3/2}f+C_{3w}h\frac{\tilde{w}}{\tilde{k}}P_k+\rho hP_{wv}+\bar{S}_w \qquad (13)$$

where $\bar{S}_k$ and $\bar{S}_w$ are the source-sink terms; function $f=1+C'_{2w}(\partial L/\partial x_i)$ and L is the characteristic distance of turbulence; Ω stands for mean movement vorticity. In $\tilde{k}-\tilde{w}$ model, the turbulent viscosity is defined as:

$$\tilde{\mu}_t=\rho\tilde{k}/\tilde{w}^{1/2} \qquad (14)$$

where $\tilde{w}$ is depth-averaged time-mean-square vorticity fluctuation of turbulence. The transport equations (the $\tilde{k}$ -eq. and $\tilde{w}$ -eq.) should be solved in the model as well. The values of empirical constants C_μ, σ_k, σ_w, C_{1w}, C_{2w}, C'_{2w} and C_{3w} are the same as those of 'standard' *k-w* model, *i.e.*, equal 0.09, 1.0, 1.0, 3.5, 0.17, 17.47 and 1.12, respectively. The corresponding additional source terms P_{kv} and P_{wv}, also mainly due to the vertical velocity gradients near the bottom, and can be expressed as:

$$P_{kv}=C_k u_*^3/h,\ P_{wv}=C_w u_*^3/h^3 \qquad (15)$$

The empirical constants C_w for open channel flow and rivers can be written as:

$$C_w=C_{2w}/\left(C_\mu^{3/2}\times C_f^{3/4}\times e^{*3/2}\right) \qquad (16)$$

The mathematical model and turbulence models, developed by the author, have been numerically investigated with laboratorial and site data for different flow situations [15, 17]. In the established mathematical model, the original empirical constants of three turbulence models suggested by their authors are employed and do not been changed never.

4 Grid Generation

In this paper, one reach of Amazon River, near the Manaus City, Brazil, has been computed by using the developed *grid-generator* and *flow-solver*, written by FORTRAN Language, where the Negro River flows into the Solimões River to form Amazon River below the Manaus City (see Figure 1). The confluent tributary, in Amazon's water system, usually has a concentration difference in comparison with the mainstream, caused by the humus in tropical rain forest (produced by tropic rains). The Negro River, however, is the largest left tributary

of Amazon River and the largest black-water river in the world. With the help of the developed software, it is possible to determine the scale of digital map (*Google Earth*), to collect conveniently geometrical data, including the positions of two curved riversides, fourteen boundaries of seven islands and the location of the tributary, and finally to generate one text file. In this file, all of messages, which illustrate necessary control variables and characteristic parameters, including those on four exterior boundaries (west inlet section, east outlet section, south and north riversides) and fourteen interior boundaries of seven islands, and can be read by *grid-generator* for generating the expectant coarse and fine grids (two levels' grids).

Fig. 1 NASA photo.

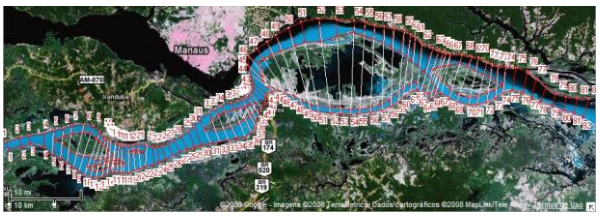

Fig. 2 *Google* map, plotted by *interface*.

Fig. 3 Coarse grid.

Fig. 4 Fine grid.

Figure 2 demonstrates the digital map, on which the developed *interface* has divided the computational river reach into 95 sub-reaches with 96 short cross-river lines (*i.e.*, NLrs=96). It is notable that the cross-river lines between the riverside and island boundary, and between the boundaries of different islands, have been redrawn, in order to involve the islands' outlines. Figure 3 presents the generated non-orthogonal body-fitted coarse grid, drawn by the grid-browser of the *interface* with the resolution of 253 nodal points in *i*-direction and 20 nodal points in *j*-direction, respectively. In the generated mesh, the nodal points in transversal grid lines are uniform. The total length of the calculated river reach is 148.404*km*. The flow direction is from the west to the east. The Negro River feeds into the mainstream on the north riverside with the numbers of nodal points from i=124 to i=127 on the coarse grid. The seven islands start at (i=19, j=12), (i=33, j=7), (i=43, j=9), (i=55, j=14), (i=86, j=11), (i=121, j=4),

(*i*=188, *j*=7) and end at (*i*=47, *j*=12), (*i*=45, *j*=7), (*i*=53, *j*=9), (*i*=61, *j*=14), (*i*=109, *j*=11), (*i*=196, *j*=4), (*i*=219, *j*=7) on the same mesh. The developed *grid-generator* generated two layers' grids, on which all of geometric data, necessary in the later calculation of flow and transport, must be stored and then can be read by the developed *flow-solver*. The resolution of the fine grid is 504×38, displayed on Figure 4. This means that one volume cell on the coarse grid was divided into four volume cells on the fine grid. Figure 5 represents the bottom topography on coarse grid, drawn by the field browser of **Q3drm1.0**. During the calculation, the variation of bottom topography was considered.

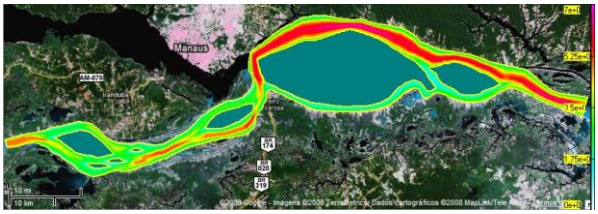

Fig. 5 Bottom topography.

5 Solutions of Flow and Side Discharge

The behaviors of flows, mixing and transport were simulated by using the developed *flow-solver*, in which the SIMPLE (*Semi-Implicit Method for Pressure-Linked Equation*) algorithm for FVA (*Finite Volume Approach*), Guass' divergence theorem, ILU (*Incomplete Lower-Upper*) decomposition, PWIM (*Pressure Weighting Interpolation Method*), SIP (*Strongly Implicit Procedure*), under relaxation and multi-grid iterative method have been used. The fundamental governing equations were solved firstly at coarse grid and then at fine grid, in the following sequence for each grid level: two momentum equations ($\overline{u}$-eq. and $\overline{v}$-eq.), one pressure-correction equation (p'-eq.), one concentration transport equation ($\overline{C_1}$-eq.), and two transport equations (*i.e.*, the $\tilde{k}$-eq. and $\tilde{\varepsilon}$-eq.; or $\tilde{k}$-eq. and $\tilde{w}$-eq.; or $\tilde{k}$-eq. and $\tilde{\omega}$-eq.), respectively.

The calculated main stream flow-rate is 15,000m^3/s, while the width, area and mean water-depth of the inlet section are 1727.54m, 7102.1m^2 and 4.11m. The empirical friction factor (C_f) equals 0.00226. The flow-rate and concentration difference of tributary are 10,000m^3/s and 100mg/L, respectively. Three depth-averaged two-equation closure turbulence models, *i.e.*, the $\tilde{k}-\tilde{\varepsilon}$, $\tilde{k}-\tilde{w}$ and $\tilde{k}-\tilde{\omega}$ models, are adopted to close the quasi 3D hydrodynamic model. The turbulent variables at the inlet sections can be calculated by empirical formulae, *i.e.*, $\tilde{k}_0$,

$\tilde{\varepsilon}_0$, $\tilde{w}_0$, $\tilde{\omega}_0$ are $0.119 m^2/s^2$, $0.00518 m^2/s^3$, $0.955/s^2$, $0.482/s$, and $\tilde{k}_{tri}$, $\tilde{\varepsilon}_{tri}$, $\tilde{w}_{tri}$, $\tilde{\omega}_{tri}$ equal $0.0575 m^2/s^2$, $0.00354 m^2/s^3$, $0.937/s^2$, $0.685/s$, respectively. On the outlet section, the variables satisfy constant gradient condition. The wall function approximation was used for determining the values of velocity components and turbulent variables at the nodal points in the vicinity of riversides and islands' boundaries.

Due to the existence of seven islands in mesh, the values of the under-relaxation factors for velocity components, pressure, concentration and two transported variables in the multi-grid iterative method are usually lower than those while no exists any island in the domain. In this example, these factors are 0.3, 0.3, 0.05, 0.7, 0.35 and 0.35, respectively. The maximum allowed numbers of inner iteration for solving velocity components, pressure, concentration and two turbulent variables are 1, 1, 20, 1, 1 and 1. The convergence criterions for inner iteration are 0.1, 0.1, 0.01, 0.1, 0.01 and 0.01, respectively. The α parameter of the Stone's solver is equal to 0.92. The normalize residuals for solving velocity field, pressure field, concentration field and the fields of two transported variables of turbulence are all less than pre-determined convergence criterion (1.e-3).

The simulation obtained various 2D and 3D distributions of flow, pressure, concentration and turbulent variables and parameters. **Q3drm1.0** provides powerful profile browser, field browser and 3D browser for plotting, printing, saving and analyzing computational results. A part of results, simulated by using three depth-averaged turbulence models on the fine grid, are presented from Figure 6 to Figure 10. Figure 6 display the results, calculated by using $\tilde{k}-\tilde{\omega}$ model and drawn by the field browser, with a: flow pattern, b: streamlines, c: color filled pressure field, d: color filled concentration field, e: color filled $\tilde{k}$ distribution and f: color filled $\tilde{\omega}$ distribution, respectively. Figure 6d illustrates that the black-water plume well develops along the left riverside at the lower reach of tributary outlet section. The distributions of the same depth-averaged physical variables and turbulent variable $\tilde{k}$, calculated by $\tilde{k}-\tilde{\varepsilon}$ and $\tilde{k}-\tilde{w}$ turbulence closure models, are similar to Figures 6a-6e. Figures 7a, 7b and 7c demonstrate the 3D distributions of $\tilde{k}$, calculated by using these three depth-averaged turbulence models and drawn by the 3D browser. They are quite similar each other, with the maximum values: $1.041 m^2/s^2$ for $\tilde{k}-\tilde{\omega}$ modeling (7a), $1.026 m^2/s^2$ for $\tilde{k}-\tilde{\varepsilon}$ modeling (7b) and $1.025 m^2/s^2$ for $\tilde{k}-\tilde{w}$ modeling (7c), respectively. Figures 8a, 8b and 8c present the 3D distributions of $\tilde{\omega}$, $\tilde{\varepsilon}$ and $\tilde{w}$, which are different each other, because of the different definitions of the used second transported variables in current computations.

Actually, the $\tilde{\varepsilon}$ value, shown in Figure 8b, ranges only from 4.746e-6 to 1.398e-2m^2/s^3; however, the $\tilde{w}$ and $\tilde{\omega}$ range from 4.862e-5 to 1.231/s^2 and from 0.697e-2 to 1.104/*s*, shown in Figure 8c and Figure 8a respectively. Figures 9a, 9b and 9c illustrate the 3D distributions of effective viscosity $\tilde{\mu}_{eff}$, while the depth-averaged turbulent eddy viscosity $\tilde{\mu}_t$ was calculated by using Eq. (2) for $\tilde{k}-\tilde{\omega}$ modeling (9a), Eq. (9) for $\tilde{k}-\tilde{\varepsilon}$ modeling (9b) and Eq. (14) for $\tilde{k}-\tilde{w}$ modeling (9c), respectively. Basically, they are similar each other, specially for $\tilde{k}-\tilde{\varepsilon}$ and $\tilde{k}-\tilde{w}$ modeling, while the maximum values of $\tilde{\mu}_{eff}$ are 22,316.8*Pa.s* (9b) and 22,310.3*Pa.s* (9c); but the same value for $\tilde{k}-\tilde{\omega}$ modeling is 22,536.4 *Pa.s* (9a). Figure 10 shows the distributions of the production term of turbulent kinetic energy, with the maximum values of P_k 4.271*Pa.m/s* for $\tilde{k}-\tilde{\omega}$ modeling (10a), 4.251*Pa.m/s* for $\tilde{k}-\tilde{\varepsilon}$ modeling (10b) and 4.246*Pa.m/s* for $\tilde{k}-\tilde{w}$ modeling (10c). They are also similar each other. Figure 11 displays the comparison between the fine light-blue concentration contour with 35*mg/L*, calculated by $\tilde{k}-\tilde{\omega}$ model closure and plotted by the field browser of **Q3drm1.0**, and the outline of black-water plume, shown on the *Google* satellite map. In this figure, the coarse yellow lines demonstrate the outline of computational domain and islands. It is clear that the simulated depth-averaged concentration contour, however, is well coincident with the outline of black-water plume. Figure 12a and 12b display the comparisons of concentration profiles along the centers of the volume cells at *i* from 1 to 504 and *j*=36 (*i.e.*, along a curved line from the inlet to the outlet near the north riverside) and at *i*=480 and *j* from 1 to 38 (*i.e.*, along a transversal section of *i*=480) on the fine grid, calculated by the depth-averaged $\tilde{k}-\tilde{\varepsilon}$, $\tilde{k}-\tilde{w}$ and $\tilde{k}-\tilde{\omega}$ turbulence models, respectively. Figure 13a and 13b show that the comparisons between $\tilde{\varepsilon}$, $\tilde{w}$ and $\tilde{\omega}$ at the same centers of the fine grid. It is well known that the orders of magnitudes of $\tilde{\varepsilon}$, $\tilde{w}$ and $\tilde{\omega}$, used in three turbulence models, have significant differences indeed.

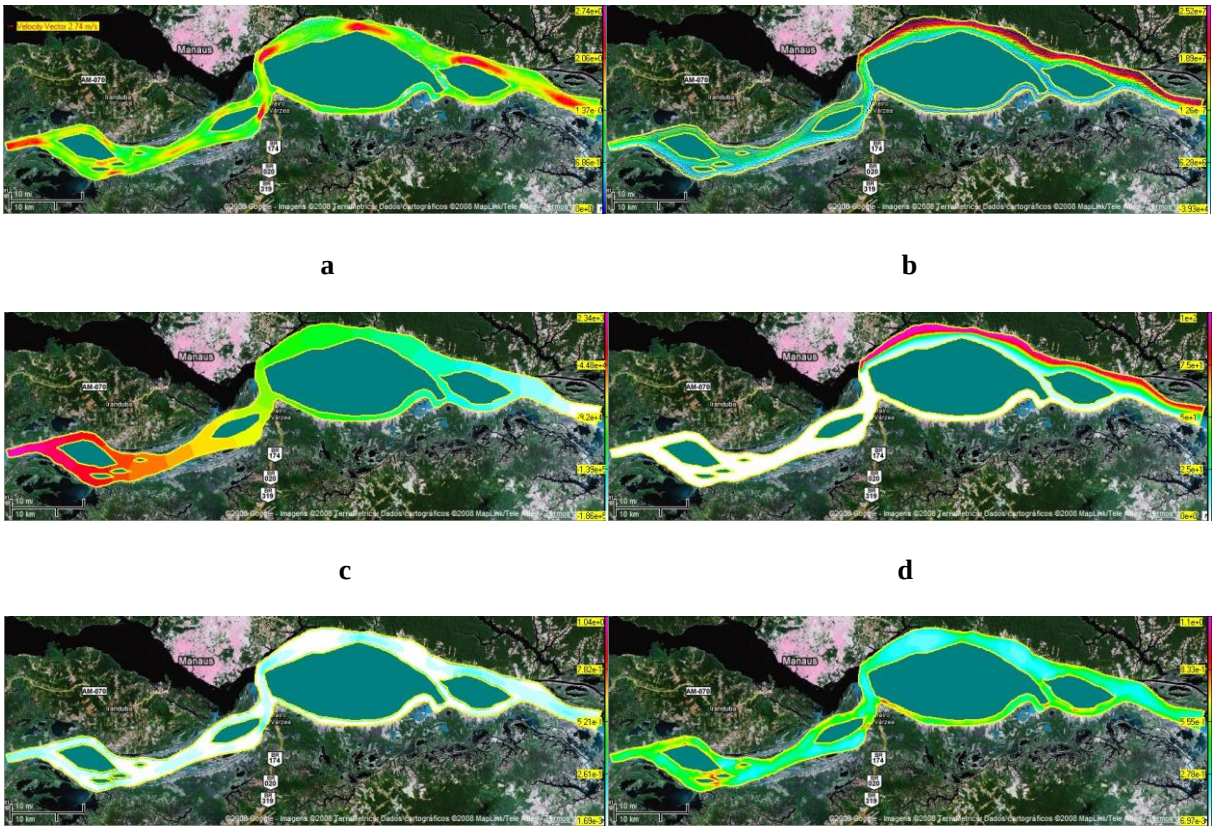

a **b**

c **d**

e **f**

Fig. 6 A part of results, calculated by $\tilde{k}-\tilde{\omega}$ model.

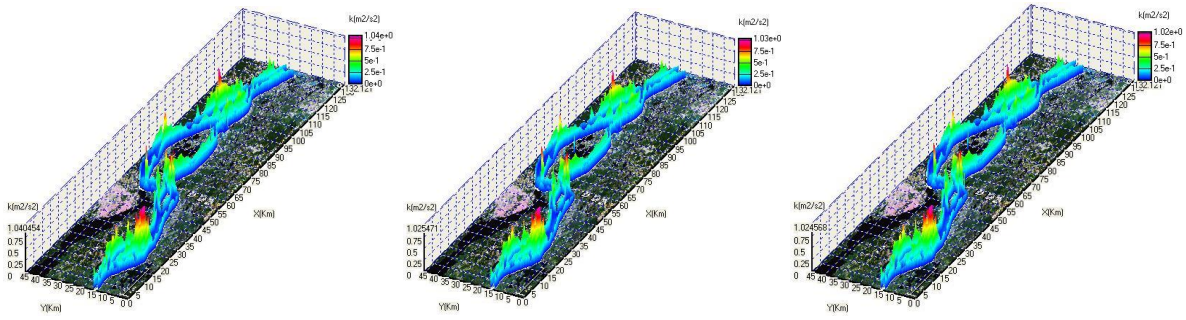

a **b** **c**

Fig. 7 3D $\tilde{k}$ distributions, calculated by $\tilde{k}-\tilde{\omega}$, $\tilde{k}-\tilde{\varepsilon}$ and $\tilde{k}-\tilde{w}$ models.

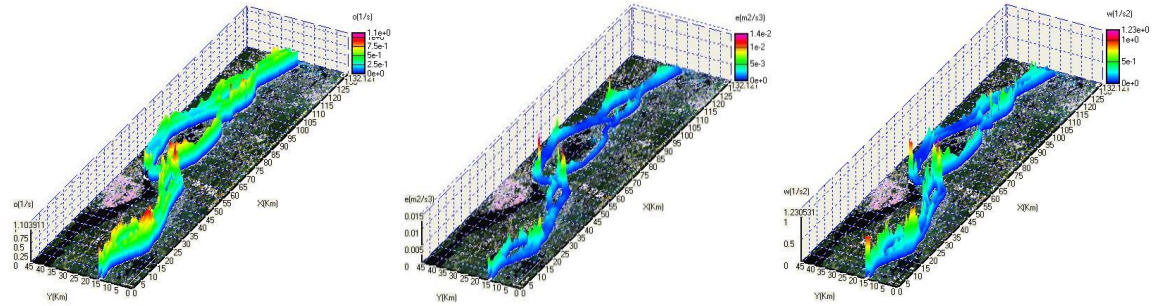

a **b** **c**

Fig. 8 3D $\tilde{\omega}$, $\tilde{\varepsilon}$ and $\tilde{w}$ distributions.

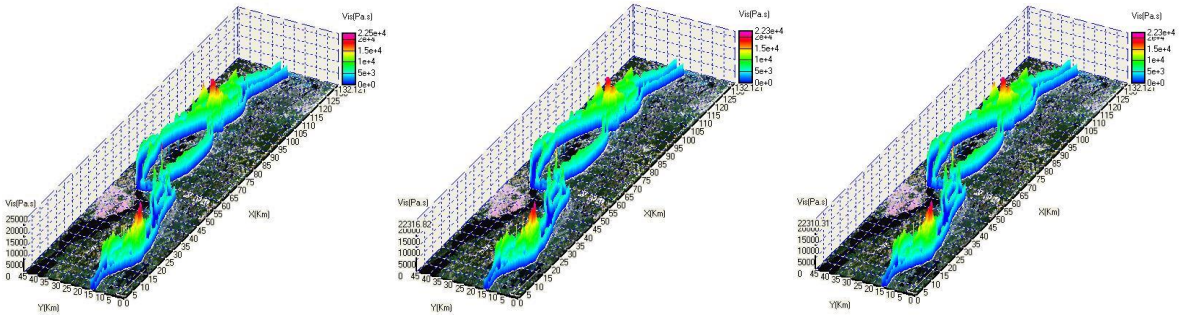

a **b** **c**

Fig. 9 3D $\tilde{\mu}_{eff}$ distributions, calculated by $\tilde{k}-\tilde{\omega}$, $\tilde{k}-\tilde{\varepsilon}$ and $\tilde{k}-\tilde{w}$ models.

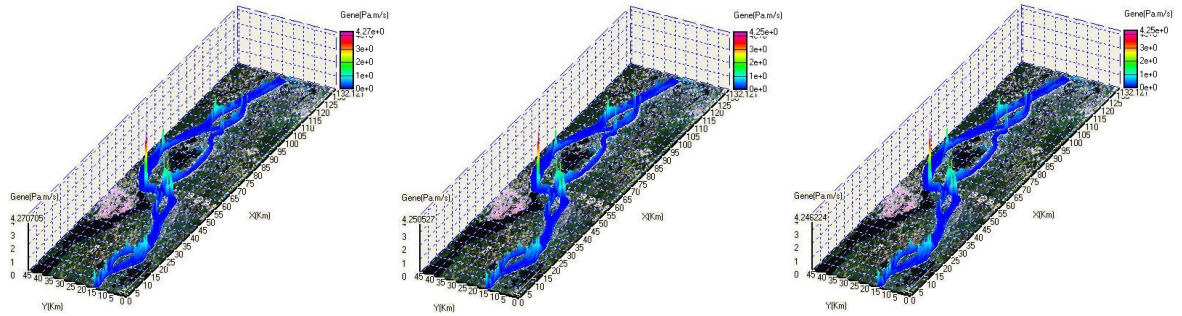

a **b** **c**

Fig. 10 P_k distributions, calculated by $\tilde{k}-\tilde{\omega}$, $\tilde{k}-\tilde{\varepsilon}$ and $\tilde{k}-\tilde{w}$ models.

Fig. 11 Comparison between calculated concentration contour and black-water plume outline.

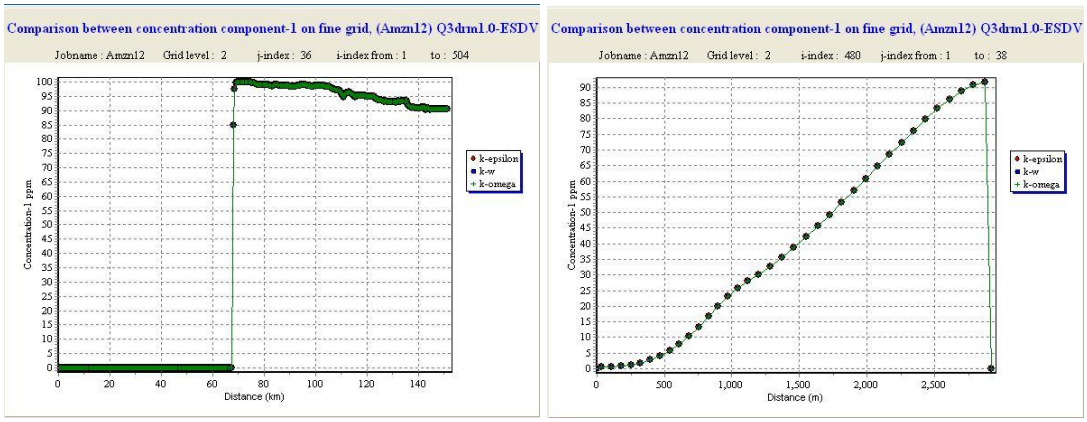

a **b**

Fig. 12 Concentrations at a: *i* from 1 to 504 and *j*=36; b: *i*=480 and *j* from 1 to 38.

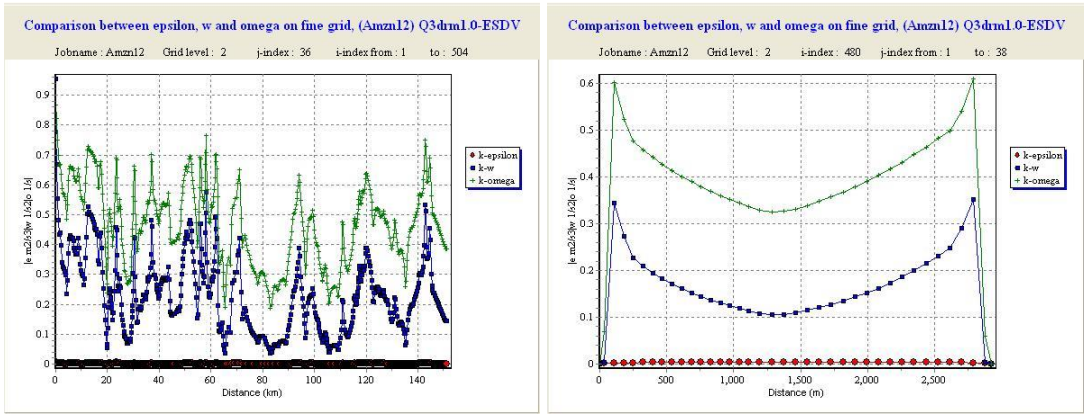

a **b**

Fig. 13 $\tilde{\omega}$, $\tilde{\varepsilon}$ and $\tilde{w}$ at a: i from 1 to 504 and j=36; b: i=480 and j from 1 to 38.

6 Black-Water Plume Development at the Beginning of Discharge

In order to well understand the development process of black-water plume, a special simulation was performed by using $\tilde{k}-\tilde{\omega}$ model for the case described as follows. Supposing the black-water concentration of the Negro River firstly to equal zero, and then, the value of concentration instantaneously reaches 100*mg/L* at *Time*=0, while the flow-rates, either of main stream or of tributary, keep constant. Figures 14a-h illustrate the plume development and variation in the lower reach of tributary outlet section, where Figure 14a presents the situation of clean water confluence; Figures 14b-h display the process of black-water inpouring and plume development, with an equal time difference Δt each other.

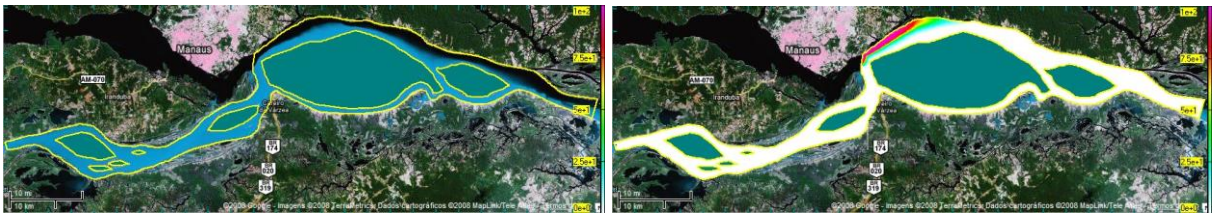

a Case 1, *ΔC=0, Time*=0 **b Case 2, ΔC=*100mg/L, Time=Δt***

c Case 3, ΔC=100mg/L, Time=2Δt **d Case 4, ΔC=100mg/L, Time=3Δt**

e Case 5, ΔC=100mg/L, Time=4Δt **f Case 6, ΔC=100mg/L, Time=5Δt**

g Case 7, ΔC=100mg/L, Time=6Δt **h Case 8, ΔC=100mg/L, Time=7Δt**

Fig. 14 Black-water plume development.

7 Discussions and Conclusions

Two-equation turbulence models are one of the most common types of RANS-based models. The so-called 'standard' two-equation closure turbulence models, widely adopted in industry, cannot be directly used in quasi 3D modeling. Till now, the vast majority of quasi 3D numerical tools by using two-equation closure approach in the world for solving hydrodynamic fundamental governing equations only can provide depth-averaged $\tilde{k}-\tilde{\varepsilon}$ turbulence model for users, which appears already beyond 30 years. However, current advanced *Computational Fluid Dynamics* (CFD) software for 'standard' 2D and 3D modeling

can provide several, even up to dozens of two-equation closure turbulence models, because there is non-existent a 'universal' turbulence closure model in the theory of turbulence modeling. Moreover, two-equation turbulence models are also very much still an active area of research and new refined two-equation models are still being developed. This situation should be changed as soon as possibly.

At present, the *k*-ω model, just like the *k*-ε model, has become industry standard model and is commonly used for most types of engineering problems. Therefore, the establishment of depth-averaged $\tilde{k}-\tilde{\omega}$ turbulence model and numerical investigation, as well as comparison with existing depth-averaged turbulence models presented in this paper, are quite significant.

Two levels' grids, one coarse mesh and one fine mesh, were used in this study. The simulation on these two grids can satisfy the computational demands. If it is necessary, by setting the number of grid levels at three, for example, the computations not only on coarse and fine grids but also on finest grid can then be realized. The selection of the number of grid levels depends on the solved problem and corresponding computational requirements.

The solved depth-averaged concentration variable in the current computation is the concentration difference of humus between the black-water from the confluent tributary and the clean water of the main stream (100*mg/L*). However, other contaminant indexes of the discharged black-water, such as COD and BOD, also can be considered as the solved variable. The developed software possesses the ability to simultaneously solve two concentration components in once calculation, which may be caused by industrial, domestic, and natural discharges.

Figure 7 demonstrates that the distributions of turbulent variable $\tilde{k}$, calculated by three turbulence models, vary strongly in the computational domain, but quite similar to one another. However, the characteristics of the distributions of $\tilde{\omega}$, $\tilde{\varepsilon}$ and $\tilde{w}$, shown in Figures 8a, 8b and 8c, respectively, are different from one another, though they also vary sharply. The calculated effective viscosity $\tilde{\mu}_{eff}$, presented in Figures 9a, 9b and 9c, also varies strongly. In fact, the eddy viscosity changes from point to point in the computational domain, especially in the areas near riversides and islands' boundaries. To solve the problems of contaminant transport caused by side discharge, for example, the plume usually develops along a region near riverside (see Figure 6d, Figure 11 and Figure 14), where $\tilde{\mu}_t$ (or $\tilde{\mu}_{eff}$) actually varies much strongly (see Figure 9). This means that $\tilde{\mu}_t$ should be precisely calculated using suitable

higher-order turbulence closure models with higher precision, and cannot be considered as an adjustable constant.

Figure 12 shows that the computational concentration profiles along the north riverbank, either calculated by $\tilde{k}-\tilde{\omega}$ and $\tilde{k}-\tilde{\varepsilon}$ closures, or calculated by $\tilde{k}-\tilde{w}$ closure, only have a quite small difference from one another. This means that the three utilized depth-averaged two-equation closure turbulence models almost have the same ability to simulate plume distributions along riverbank. This conclusion also coincides with the result of author's previous research that the depth-averaged two-equation closure turbulence closure models are suitable for modeling strong mixing turbulence [17]. However, the abilities and behaviors of different depth-averaged two-equation closure turbulence models for rather weak mixing, also often encountered in engineering, should be further investigated.

Except for the different definitions of transported variables: $\tilde{\varepsilon}$, $\tilde{w}$ and $\tilde{\omega}$, the order of magnitude of $\tilde{\varepsilon}$ is smaller than the order of magnitude of $\tilde{w}$, and much smaller than the order of magnitude of $\tilde{\omega}$. It should be noticed that three transported variables: $\tilde{\varepsilon}$, $\tilde{w}$ and $\tilde{\omega}$ all appear in the denominators of Eqs. (9), (14) and (2), which were used to calculate turbulent eddy viscosity $\tilde{\mu}_t$. For numerical simulation, the occurrence of numerical error is unavoidable, especially in the region near irregular boundary. It is clear that a small numerical error, caused by solving $\tilde{\varepsilon}$-eq, for example, will bring on larger error for calculating eddy viscosity than the same error caused by solving the other two equations (*i.e.*, the $\tilde{w}$-eq. and $\tilde{\omega}$-eq.). Without doubt, the elevation of the order of magnitude of the used second turbulent variable, reflecting the advance of two-equation turbulence models, provides a possibility for users to improve their computational precision. The insufficiency of traditional depth-averaged $\tilde{k}-\tilde{\varepsilon}$ turbulence model may be avoided by adopting other turbulence models that have appeared recently, such as the $\tilde{k}-\tilde{\omega}$ model.

The developed *Graphical User Interfaces* of **Q3drm1.0** and **Q3drm2.0** software can be used in various Windows-based microcomputers. The pre- and post-processors of this numerical tool, supported by a powerful self-contained map support tool together with a detailed help system, can help the user to easily compute the flows and transport behaviors in natural waters, closed by using three different depth-averaged two-equation turbulence models, and to plot and analyze various 2D and 3D graphics of computed results.

Acknowledgement

The partial support of FAPESP through the Process No. PIPE 2006/56475-3 is gratefully acknowledged.

References

[1] M. Choi, H. Takashi, A numerical simulation of lake currents and characteristics of salinity changes in the freshening process, J. Japan Society of Hydrology and Water Resources, 13 (2000) 439-452. (in Japanese)

[2] M. Lunis, V.I. Mamchuk, V.T. Movchan, L.A. Romanyuk, E.A. Shkvar, Algebraic models of turbulent viscosity and heat transfer in analysis of near-wall turbulent flows, International J. of Fluid Mechanics Research, 31 (2004) 60-74. http://dx.doi.org/doi/10.1615/InterJFluidMechRes.v31.i3.60

[3] E. Viparelli, O.E. Sequeiros, A. Cantelli, P.R. Wilcock, G. Parker, River morphodynamics with creation/consumption of grain size stratigraphy 2: numerical model, Journal of Hydraulic Research. 48 (2010) 727-741. http://dx.doi.org/doi/doi:10.1080/00221686.2010.526759

[4] W. Rodi, R.N. Pavlovic, S.K. Srivatsa, Prediction of flow pollutant spreading in rivers, In: H.B. Fischer (ed.), Transport Models for Inland and Coastal Waters, University of California Academic Press, 1980, pp. 63-111.

[5] L. Cea, L. Pena, J. Puertas, M.E. Vázquez-Cendón ME, E. Peña, Application of several depth-averaged turbulence models to simulate flow in vertical slot fishways, J. Hydraulic Engineering. 133 (2007) 160-172. http://dx.doi.org/doi/10.1061/(ASCE)0733-9429(2007)133:2(160)

[6] I. Kimura, W.S.J. Uijttewaal, T. Hosoda, M.S. Ali, URANS computations of shallow grid turbulence. J. Hydraulic Engineering, 135 (2009) 118-131. http://dx.doi.org/doi/10.1061/(ASCE)0733-9429(2009)135:2(118)

[7] J.T. Lee, H.C. Chan, C.K. Huang, Y.M. Wang, W.C. Huang, A depth-averaged two-dimensional model for flow around permeable pile groins, International J. the Physical Sciences. 6 (2011) 1379-1387. http://dx.doi.org/doi/10.5897/IJPS11.078

[8] http://www.cfd-online.com/Wiki/Turbulence_modeling

[9] P.G. Saffman, A model for inhomogeneous turbulent flow, Proc. Roy. Soc., A317 (1970) 417-433.

[10] D.C. Wilcox, Turbulence Modeling for CFD, La Canada, DCW Industries, Inc., 1998.

[11] J.H. Ferziger, M. Peric, Computational Methods for Fluid Dynamics, 3rd ed., Berlin, 2002.

[12] A. Riasi, A. Nourbakhsh, M. Raisee, Unsteady turbulent pipe flow due to water hammer using k–ω turbulence model, J. of Hydraulic Research. 47 (2009) 429-437. http://dx.doi.org/doi/ 10.1080/00221681003726247

[13] L.R. Yu, J. Yu, Numerical research on flow and thermal transport in cooling pool of electrical power station using three depth-averaged turbulence models, Water Science and Engineering, 2(2009) 1-12. http://dx.doi.org/doi/10.3882/j.issn.1674-2370.2009.03.001

[14] J.J. McGuirk, W. Rodi, A Depth-Averaged Mathematical Model for Side Discharges into Open Channel Flow, SFB 80/T/88, Universität Karlsruhe, 1977.

[15] L.R. Yu, S.N. Zhang, A new depth-averaged two-equation ($\tilde{k}-\tilde{w}$) turbulent closure model, J. of Hydrodynamics B1 (1989) 47-54.

[16] J.O. Ilegbusi, D.B. Spalding, Application of a New Version of the k-w Model of Turbulence to a Boundary Layer with Mass Transfer, CFD/82/15, Imperial College, 1982.

[17] L.R. Yu, A.M. Righetto, Depth-averaged turbulence $\tilde{k}-\tilde{w}$ model and applications, Advances in Engineering Software, 32 (2001) 375-394. http://dx.doi.org/doi/10.1016/S0965-9978(00)00100-9